

e^+e^- pairs from π^-A reactions *

Th. Weidmann, E. L. Bratkovskaya, W. Cassing, and U. Mosel

Institut für Theoretische Physik, Universität Giessen

D-35392 Giessen, Germany

Abstract

We present a dynamical study of e^+e^- production in π^-A reactions at 1.3 and 1.7 GeV on the basis of the Coupled-Channel-BUU approach. The contributions from vector mesons (ρ, ω) are calculated taking into account the collisional broadening effect and are compared to background sources in the dilepton spectrum from the Dalitz decays of ω and η mesons produced in the reaction. Two possible scenarios for the medium modifications of the vector mesons are investigated, i.e. the 'dropping mass' scheme for the ρ and ω and a momentum dependent ρ -meson spectral function that includes the polarization of the ρ -meson due to resonant $\rho - N$ scattering.

PACS: 25.80.-e, 25.80.Hp

Keywords: leptons, pion induced reactions

*Work supported by BMBF and GSI Darmstadt.

I. INTRODUCTION

The properties of hadrons in the nuclear medium are of fundamental interest (cf. Refs. [1–5]). According to QCD sum rules [4–6] or QCD inspired effective Lagrangian models [1–3,7–13] the properties of the vector mesons (ρ , ω and ϕ) should change with the nuclear density. Furthermore, along with a dropping mass the phase space for the resonance decay also decreases which results in a modification of the resonance lifetime in matter. On the other hand, due to collisional broadening – which depends on the nuclear density and the resonance-nucleon interaction cross section (cf. Refs. [14,15]) – the resonance lifetime decreases again.

The in-medium properties of vector mesons have been studied experimentally so far by dilepton measurements at SPS energies for proton-nucleus and nucleus-nucleus collisions [16–19]. As proposed by Li, Ko, and Brown [20] and Ko et al. [21], the observed enhancement in $A + A$ reactions compared to $p + A$ collisions in the invariant mass range $0.3 \leq M \leq 0.7$ GeV might be due to a shift of the ρ -meson mass following Brown/Rho scaling [1] or the Hatsuda and Lee sum rule prediction [4]. The microscopic transport studies in Refs. [22–24] for these systems support these results [20,21].

However, also a more conventional approach including the change of the ρ -meson spectral function in the medium due to the coupling of ρ , π , Δ and nucleon dynamics along the lines of Refs. [7–10] was found to be (roughly) compatible with the CERES data [10,22]. Meanwhile, our knowledge on the ρ spectral function has improved since – as first pointed out by Friman and Pirner [11] – resonant ρ - N interactions significantly enhance the strength in the vector-isovector channel at low invariant mass; this has also been confirmed recently in Ref. [13] where the authors find a significant smearing of the ρ strength at low ρ momenta due to a selfconsistent evaluation of the resonance widths. In fact, the CERES data for $S + Au$ at 200 A GeV and $Pb + Au$ at 160 A GeV, using an expanding fireball model, were found to be compatible with such a hadronic scenario [12].

Recently, the thermodynamical result of Ref. [12] was supported by Hadron String Dy-

namics (HSD) transport calculations [25] where an improved ρ spectral function was used. The conclusion in Ref. [25] was that both the 'dropping mass' scenario [21–24] as well as the hadronic spectral function approach [12] lead to dilepton spectra which are in good agreement with the experimental data for all systems at SPS energies. A similar analysis was done also for BEVALAC/SIS energies [26] (where quite different temperature and density regimes are probed) involving both the spectral functions from Refs. [12,13]. It was found that these spectral functions give practically the same result for dilepton spectra at BEVALAC/SIS energies.

Additional, and possibly more sensitive, information could be provided by studies using more elementary probes such as pions or protons as incoming particles. In such reactions the nuclear density ($\leq \rho_0$) is obviously lower than in heavy-ion collisions, but the phase-space distribution of the nuclear matter is almost stationary and much better known. In case of pion-nucleus reactions the ω meson can be produced with low momenta in the laboratory system such that a substantial fraction of them will also decay inside a heavy nucleus [27–29]. In Refs. [28,29], which employed the Hatsuda-Lee mass shift [4], it was shown on the basis of the intranuclear cascade (INC) approach that the mass distributions of the vector mesons decaying inside the nucleus have a two-component structure [15] in the dilepton invariant mass spectrum: the first, high-mass component corresponds to resonances decaying in the vacuum, thus showing the free spectral function which is very narrow in case of the ω meson; the second (broader) component of lower masses corresponds to the resonance decay inside the nucleus.

The many detailed hadronic model studies quoted above have shown that the assumption of a very narrow, unchanged width of the vector mesons, that underlies the Hatsuda-Lee prescription, is oversimplified. This has also recently been discussed in Ref. [6], where the authors have shown that QCD sum rules pose only very loose constraints on the in-medium properties of vector mesons.

In this paper we, therefore, report results of detailed microscopic calculations on the basis of the Coupled-Channel-Boltzmann-Uehling-Uhlenbeck (CBUU) model [30] for the dilepton

production in π^-C , π^-Ca , π^-Pb collisions at kinetic energies $E_{kin} = 1.3$ and 1.7 GeV employing also a realistic spectral function for the ρ meson [13] in addition to the collisional broadening and 'dropping' mass effects of vector mesons studied in Refs. [28,29]. Within this transport model it is possible to investigate simultaneously $\gamma + A$, $\pi + A$, $p + A$ and $A + A$ reactions in a wide dynamical range such that especially the pion dynamics can be controlled by a large set of independent experiments [30].

Our paper is organized as follows: In Section 2 we briefly describe the CBUU transport approach and its implementation for pion-induced reactions, the πN total reaction cross section and the elementary processes for meson production and their interactions employed in the CBUU approach. In Section 3 we discuss the elementary channels for dilepton production and collisional broadening and the in-medium modification schemes ('dropping' mass and ρ spectral function approach) which will be applied for calculating the dilepton spectra. Section 4 contains a detailed study of dilepton spectra for π^-C , π^-Ca , π^-Pb reactions at $E_{kin} = 1.3$ and 1.7 GeV. We close with a summary in Section 5.

II. INGREDIENTS OF THE CBUU-MODEL

A. Binding energy and nuclear stability

The dynamical description of pion-nucleus collisions is performed within the Coupled-Channel-BUU approach [30] which has been found to describe reasonably well various pion data at SIS energies. The model has been described in detail in [30]; here we briefly recall the main ingredients.

In line with Refs. [31–34] the dynamical evolution of heavy-ion collisions or hadron-nucleus reactions below the pion-production threshold is described by a transport equation for the nucleon one-body phase-space distribution function $f_N(\mathbf{r}, \mathbf{p}, t)$,

$$\begin{aligned} \frac{\partial f(\mathbf{r}, \mathbf{p}, t)}{\partial t} + \left\{ \frac{\mathbf{p}}{E} + \frac{m^*(\mathbf{r}, \mathbf{p})}{E} \nabla_p U(\mathbf{r}, \mathbf{p}) \right\} \nabla_r f(\mathbf{r}, \mathbf{p}, t) \\ + \left\{ -\frac{m^*(\mathbf{r}, \mathbf{p})}{E} \nabla_r U(\mathbf{r}, \mathbf{p}) \right\} \nabla_p f(\mathbf{r}, \mathbf{p}, t) = I_{coll}[f(\mathbf{r}, \mathbf{p}, t)], \end{aligned} \quad (1)$$

where \mathbf{r} and \mathbf{p} denote the spatial and the momentum coordinate of the nucleon, respectively, while N stands for a proton (p) or neutron (n). The effective mass $m^*(\mathbf{r}, \mathbf{p})$ in Eq. (1) includes the nucleon restmass $m_N (= 938 \text{ MeV}/c^2)$ as well as a scalar momentum-dependent mean-field potential $U(\mathbf{r}, \mathbf{p})$,

$$m^*(\mathbf{r}, \mathbf{p}) = m_N + U(\mathbf{r}, \mathbf{p}) \quad (2)$$

for the baryons. The nucleon quasi-particle dispersion relation then is

$$E(\mathbf{r}, \mathbf{p}) = \sqrt{m^*(\mathbf{r}, \mathbf{p})^2 + \mathbf{p}^2}. \quad (3)$$

We note that we have neglected an explicit vector interaction due to numerical reasons in order to achieve a better stability of nuclei in their 'groundstate'. However, this is of no concern since the vector interaction plays no role in $\pi + A$ reactions as considered in this work.

Here we employ the momentum-dependent mean-field potential proposed by Welke et al. [35] with an additional isospin symmetry potential U^{symm} , i.e.

$$U^{nr}(\mathbf{r}, \mathbf{p}) = A \frac{\rho}{\rho_0} + B \frac{\rho^\tau}{\rho_0} + 2 \frac{C}{\rho_0} \int d^3 p' \frac{f(\mathbf{r}, \mathbf{p}')}{1 + \left(\frac{\mathbf{p}-\mathbf{p}'}{\Lambda}\right)^2} + U^{symm}, \quad (4)$$

where U^{symm} is

$$U^{symm} = D \frac{\rho_p(\mathbf{r}) - \rho_n(\mathbf{r})}{\rho_0} \tau_z, \quad (5)$$

with $\tau_z = -1$ for neutrons and $\tau_z = +1$ for protons; for the strength of the symmetry potential we use $D = 30 \text{ MeV}$ in line with [36].

As an extension of the momentum-independent Skyrme type potentials for nuclear matter [33,35] the parametrization (4) has no manifest Lorentz-properties. However, definite Lorentz-properties are required for a transport model at relativistic energies. To achieve this goal we evaluate the non-relativistic mean-field potential U^{nr} in the local rest frame (LRF) of nuclear matter which is defined by the frame of reference with vanishing local vector baryon current ($\mathbf{j}(r, t) = \mathbf{0}$). Assuming only scalar potentials in the LRF we then equate

the expressions for the single-particle energies using the non-relativistic potential U^{nr} and the scalar potential U by

$$\sqrt{p^2 + m^2} + U^{nr}(\mathbf{r}, \mathbf{p}) = \sqrt{p^2 + (m + U(\mathbf{r}, \mathbf{p}))^2}. \quad (6)$$

Eq. (6) now allows to extract the scalar mean-field potential $U(\mathbf{r}, \mathbf{p})$ which we will use throughout our calculations for the baryons.

For our calculations we use a (momentum-dependent) equation of state (EOS) for nuclear matter with an incompressibility of $K = 290$ MeV (i.e. $A = -29.3$ MeV, $B = 57.2$ MeV, $C = -63.5$ MeV, $\tau = 1.760$, $\Lambda = 2.13$ fm $^{-1}$). For the pion-nucleus reactions to be investigated in this study, however, the nuclear incompressibility K is no decisive quantity and is only quoted for completeness.

For $\pi + A$ reactions it is important that the nuclear groundstate properties, i.e. density and binding energies, are well reproduced. We illustrate the quality of our groundstate in Fig. 1, where we show the binding energy per nucleon as a function of the nucleon number A . The solid curve corresponds to the binding energy calculated with U^{symm} whereas the dashed curve is the result without the isospin symmetry potential; the solid curve belongs to nuclei that are quite stable over time periods longer than the typical reaction time of 15 fm/c in case of a Pb-target. Comparing our calculations for stationary nuclei with the empirical liquid drop result (dotted line) we find that our dynamical calculations with U^{symm} agree reasonably well with the experimental systematics.

In the CBUU-model we explicitly propagate the mesonic degrees of freedom π , η , ρ and a scalar meson σ that simulates correlated 2π pairs in the isospin 0-channel. Besides the nucleon and the $\Delta(1232)$ we, furthermore, include all baryonic resonances up to a mass of 1950 MeV/c 2 : i.e. $N(1440)$, $N(1520)$, $N(1535)$, $\Delta(1600)$, $\Delta(1620)$, $N(1650)$, $\Delta(1675)$, $N(1680)$, $\Delta(1700)$, $N(1720)$, $\Delta(1905)$, $\Delta(1910)$ and $\Delta(1950)$; the resonance properties are adopted from the PDG [37].

Denoting the nucleon by N and the baryon resonances listed above by R and R' , we include the following channels:

- elastic baryon-baryon collisions $NN \leftrightarrow NN, NR \leftrightarrow NR$;
- inelastic baryon-baryon collisions $NN \leftrightarrow NR, NR \leftrightarrow NR', NN \leftrightarrow \Delta(1232)\Delta(1232)$;
- inelastic baryon-meson reactions $R \leftrightarrow N\pi, R \leftrightarrow N\pi\pi, \Delta(1232)\pi, N(1440)\pi, N\rho, N\sigma$;
 $N(1535) \leftrightarrow N\eta; NN \leftrightarrow NN\pi$;
- meson-meson collisions $\rho \leftrightarrow \pi\pi$ (p-wave), $\sigma \leftrightarrow \pi\pi$ (s-wave)

B. πN total reaction cross sections

In order to describe pion-baryon scattering in the framework of the resonance picture a Breit-Wigner formulation for the cross sections (eq. $\pi N \rightarrow mN$) was used

$$\sigma_{ab \rightarrow R \rightarrow cd} = \frac{2J_R + 1}{(2S_a + 1)(2S_b + 1)} \frac{4\pi}{p_i^2} \frac{s \Gamma_{R \rightarrow ab} \Gamma_{R \rightarrow cd}}{(s - M_R^2)^2 + s \Gamma_{tot}^2}. \quad (7)$$

In Eq. (7) ab and cd denote the baryon and the meson in the initial and final state of the reaction and R is the intermediate baryon resonance. J_R , S_a and S_b are the spins of the baryon resonance and the particles in the initial state of the reaction, while $\Gamma_{R \rightarrow ab}$, $\Gamma_{R \rightarrow cd}$ are taken from the PDG [37] and p_i^2 stands for the squared momentum of the incoming meson in the resonance rest frame.

The solid line in Fig. 2 shows the total $\pi^- - p$ -cross section within the CBUU model in comparison to the experimental data from [38]. To calculate this cross section we replace the partial widths $\Gamma_{R \rightarrow cd}$ in Eq. (7) by the total widths of the baryonic resonances and sum up the contributions from all resonances incoherently. The dot-dot-dashed, the dot-dashed and the short-dashed lines in Fig. 2 show the contributions from the $\Delta(1232)$, the $N(1440)$ and the $N(1520)$ separately. We supplement the resonances included in Ref. [30] with an additional effective two-pion production channel (long-dashed line) in order to reproduce properly the total cross section data at high $s^{1/2}$ which is quite essential for $\pi + A$ reactions in the energy regime considered. By using alternatively an effective resonance with a one-pion decay width we have ascertained that our results are independent of the specific way in which the missing pion strength at high energies is corrected.

C. Elementary processes for meson production and meson-baryon interactions

Because of the small cross sections involved we can treat the production of vector mesons (ρ, ω) and η 's perturbatively. Since we work within the parallel ensemble algorithm, each parallel run of the transport calculation can be considered approximately as an individual reaction event, where binary reactions in the entrance channel at given invariant energy \sqrt{s} lead to final states with 2 or 3 particles with a relative weight W_i for each event i . W_i is defined by the ratio of the production cross section to the total hadron-hadron cross section¹. The perturbative treatment implies that the initial hadrons are not modified in their respective final channels. On the other hand, each perturbative particle is represented by a testparticle with weight W_i and propagated according to the Hamilton equations of motion. Elastic and inelastic reactions with baryons are computed in the standard way [39]. The final cross section is obtained by multiplying each testparticle with its weight W_i . In this way one achieves a time-saving simulation of the vector meson production, propagation and reabsorption during the pion-nucleus collision.

The η mesons are produced in pion-baryon and baryon-baryon collisions according to the elementary production cross sections from Refs. [40,41]. However, in the present analysis we assume the $pn \rightarrow pn\eta$ cross section to be about 6 times larger than the $pp \rightarrow pp\eta$ cross section close to threshold in line with the new data from the WASA collaboration [42].

For the vector mesons (ρ, ω) we have to take into account the pion-baryon production channels $\pi^- p \rightarrow \omega n, \pi^- N \rightarrow \omega X, \pi^- p \rightarrow \rho n, \pi^- N \rightarrow \rho X$ and in addition to [28,29] the baryon-baryon channels $BB \rightarrow \rho BB, BB \rightarrow \rho X, BB \rightarrow \omega BB, BB \rightarrow \omega X$.

For the exclusive process $\pi^- p \rightarrow \omega n$ we use a parametrization of the experimental data from Ref. [43]:

¹The actual final states are chosen by Monte Carlo sampling according to the 2 or 3-body phase space.

$$\sigma_{\pi^-p \rightarrow \omega n}^{excl.} = C \frac{p_{\pi N} - p_{\omega}^0}{p_{\pi N}^{\alpha} - d}, \quad (8)$$

where $p_{\pi N}$ is the relative momentum (in GeV/c) of the pion-nucleon pair while $p_{\omega}^0 = 1.095$ GeV/c is the threshold value. The parameters $C = 13.76$ mb (GeV/c) $^{\alpha-1}$, $\alpha=3.33$ and $d=1.07$ (GeV/c) $^{\alpha}$ describe satisfactorily the data on the energy-dependent cross section in the near-threshold energy region. For ρ^0 -meson production $\pi^-p \rightarrow \rho n$ we use the same cross section as for the ω -meson; this holds experimentally within 20%.

For the inclusive vector meson production $\pi^-p \rightarrow VX$, $V = \omega, \rho$ we use the parametrization from Ref. [44]

$$\sigma_{\pi^-p \rightarrow VX}^{incl.} = a_V (x-1)^{b_V} x^{-c_V}, \quad (9)$$

where the scaling variable is defined as $x = s/s_{th}$, $s_{th} = (m_N + m_V)^2$. For ω -production we have $a_{\omega} = 4.8$ mb, $b_{\omega} = 1.47$, $c_{\omega} = 1.26$; for ρ -production we have $a_{\rho} = 3.6$ mb, $b_{\rho} = 1.47$, $c_{\rho} = 1.26$ using $m_{\rho} = 0.77$ GeV in the vacuum case. In the actual calculation we take the maximum of the parametrizations (9) and (8). These cross sections have been shown in Ref. [44] to reproduce the available data very well.

For the vector meson production in baryon-baryon channels (this contribution is quite small for π^-A reactions) we also use the parametrization from Ref. [44]

$$\sigma_{pp \rightarrow VX}^{incl.} = a_V (x-1)^{b_V} x^{-c_V}, \quad (10)$$

where the scaling variable is defined again as $x = s/s_{th}$, $s_{th} = (2m_N + m_V)^2$. For ω -production we use $a_{\omega} = 2.2$ mb, $b_{\omega} = 1.47$, $c_{\omega} = 1.1$; for ρ -production we use $a_{\rho} = 2.5$ mb, $b_{\rho} = 1.47$, $c_{\rho} = 1.11$.

For the interactions of vector mesons with baryons we include the following channels: $\omega N \rightarrow \omega N$, $\omega N \rightarrow \pi N$, $\omega N \rightarrow \pi\pi N$; $\rho N \rightarrow \rho N$, $\rho N \rightarrow \pi N$, $\rho N \rightarrow \pi\pi N$. Since apart for the πN final channels no experimental data are directly available we adopt the parametrizations from Ref. [28,29]. The total ωN cross section is described as

$$\sigma_{\omega N}^{tot.}(p_{lab}) = A + \frac{B}{p_{lab}} \quad (11)$$

with $A = 11$ mb and $B = 9$ mb GeV/c. The elastic ωN cross section is parametrized as

$$\sigma_{\omega N}^{el}(p_{lab}) = A \frac{1}{1 + ap_{lab}} \quad (12)$$

with $A = 20$ mb and $a = 1$ GeV⁻¹c.

For the ρ -N total and elastic cross sections we adopt the results of Ref. [45], which were calculated within the resonance model using the experimental branching ratios for the resonances involved [37]. A good fit to the results of Ref. [45] in the energy range of interest is given by:

$$\begin{aligned} \sigma_{\rho^0 N}^{tot} &= 26.0 + 0.9 p^{-6} \text{ [mb]} \\ \sigma_{\rho^0 N}^{el} &= 13.0 + 0.25 p^{-6} \text{ [mb]}, \end{aligned} \quad (13)$$

where p [GeV/c] is the meson momentum in the cms. Since this parametrization diverges for zero momentum, we numerically include an upper limit of 200 mb for the total cross section.

The channel $\rho N \rightarrow \pi N$ is determined via detailed balance from the inverse reaction (8) whereas the ω absorption channel is described by $\sigma_{\omega N}^{abs} = \sigma_{\omega N}^{tot} - \sigma_{\omega N}^{el}$.

In order to demonstrate the relevant range of the elementary production cross sections we display in Fig. 3 the distribution in the pion-baryon collision number versus the invariant energy \sqrt{s} above the threshold for ρ production $\sqrt{s_{th}} = m_N + m_\rho$, i.e. $dN/d\sqrt{s}$ (histogram) for π^- Pb at $E_{kin} = 1.3$ GeV. The arrow indicates the incoming energy. Due to Fermi motion and secondary interactions the $dN/d\sqrt{s}$ is not a sharp peak, but a broader distribution. At the pion kinetic energy of 1.3 GeV one thus is sensitive to the elementary vector meson production cross section for excess energies of 100 – 300 MeV.

We finally note that all the vector mesons are produced and propagated with their pole mass. Their spectral functions are taken into account only in their decay to e^+e^- . However, the essential broadening of the ρ spectral function in the nuclear medium due to elastic and inelastic scattering with nucleons is taken into account dynamically, though not consistently with the model from Ref. [13].

III. DILEPTON PRODUCTION

A. Elementary channels

The dilepton production is calculated perturbatively by including the contributions from the Dalitz-decays $\Delta \rightarrow Nl^+l^-$, $N(1440) \rightarrow Nl^+l^-$, $N(1520) \rightarrow Nl^+l^-$, $N(1535) \rightarrow Nl^+l^-$, $\pi^0 \rightarrow \gamma l^+l^-$, $\eta \rightarrow \gamma l^+l^-$, $\omega \rightarrow \pi^0 l^+l^-$ and the direct dilepton decays of the vector mesons ρ and ω . For a detailed description of the Δ , N^* Dalitz decays we refer the reader to Ref. [40]; the dilepton decays of the η and vector mesons are described in Ref. [24].

The novel channel included as compared to Refs. [28,29] is the Dalitz decay of the $N(1520)$ resonance which is described in the same way as the Δ resonance with spin 3/2 (see [40]), but using a coupling constant $g = 0.96$ and $\Gamma_0 = 1.1$ MeV in Eqs. (4.8)-(4.13) in Ref. [40]. We include this resonance because its presence was recently shown to dominate the ρ -meson properties in a baryon-rich environment [13]. We also note, that compared to the INC calculations in Refs. [28,29] we employ different parametrizations for the η -production channels based on the more recent data from the WASA and PINOT Collaborations [42,46].

The dilepton radiation resulting from πN interactions is dominantly made up by two contributions. One consists of reactions in which the pion is absorbed on the nucleon to form a nucleon resonance which then later undergoes a Dalitz decay into Ne^+e^- ; these processes are explicitly contained in the transport calculations. The second class of reactions consists of those in which the pion reemerges, so that there may be bremsstrahlung from the external legs of the charged particles. In Refs. [28,29] a phase-space corrected soft photon approximation [47] for the latter processes has been adopted. However, this approximation has recently been discussed in detail by Lichard [49] and it has been shown for a particular example that various approximations, including the one used in Refs. [28,29], can lead to large uncertainties of up to a factor of about 5. This uncertainty estimate agrees with that obtained from a comparison with an 'exact' calculation from pn bremsstrahlung in Fig. 5 in Ref. [40]. Since the phase-space corrected soft photon approximation more likely provides

an upper limit for the radiation from the external legs [49,50] and the πN bremsstrahlung channel was found in Ref. [29] to be a minor background in the vector-meson mass regime, we discard an explicit calculation of this channel in this work. We note, however, that this bremsstrahlung contribution might be of similar order as the Dalitz decay of the η -meson at lower invariant masses [29]. Thus by measuring the η -yield from its 2γ -decay independently one might subtract the η Dalitz channel from the dilepton mass spectrum – as well as for the π^0 , respectively – and obtain experimental bounds on this channel, too.

B. In-medium vector mesons and collisional broadening

1. Collisional broadening

The production and propagation of short lived hadronic resonances with all their off-shell properties in the nuclear medium is presently an unsolved problem and especially the production of ρ -mesons close to threshold is uncertain since its width changes drastically in the nucleus as compared to the vacuum. We thus have to introduce a couple of simplifying assumptions for this explorative study that finally have to be controlled by experimental data. Following [28,29] we assume that (in first order) the in-medium resonance can also be described by a Breit-Wigner formula with a mass and width distorted by the nuclear environment,

$$F(M) = \frac{1}{2\pi} \frac{\Gamma_V^*}{(M - m_V^*)^2 + \Gamma_V^{*2}/4}, \quad (14)$$

containing the effects of collisional broadening,

$$\Gamma_V^* = \Gamma_V + \delta\Gamma, \quad (15)$$

where

$$\delta\Gamma = \gamma v \sigma_{VN}^{tot} \rho_N, \quad (16)$$

as well as a shift of the meson mass

$$m_R^* = m_V + \delta m_V. \quad (17)$$

In Eq. (16) v is the resonance velocity with respect to the target at rest, γ is the associated Lorentz factor, ρ_N is the nuclear density and σ_{VN}^{tot} is the meson-nucleon total cross section. For $\sigma_{\rho N}^{tot}$ we use Eq. (13) while for $\sigma_{\omega N}^{tot}$ we adopt Eq. (11). In using (15) we neglect the decrease in the width due to the lowered mass of the vector mesons which is small compared to the collisional broadening.

In Fig. 4 we show the width of ρ and ω mesons calculated dynamically according to Eqs. (15) and (16) (open squares) for π^- Pb at $E_{kin} = 1.3$ GeV. The solid lines indicate a linear fit of the form

$$\Gamma_V^*(\rho_N) = \Gamma_V^0(\rho_N) \left(1 + \beta \frac{\rho_N}{\rho_0} \right), \quad (18)$$

where $\beta = 1.55$ for the ρ -meson and $\beta = 9$ for the ω -meson. While the collisional broadening is roughly twice that of the bare ρ -width, it increases the width of the ω -meson by about one order of magnitude. The latter values imply that the lifetime of the ρ at density ρ_0 drops to ≈ 0.7 fm/c while the lifetime of the ω meson decreases to ≈ 2.7 fm/c at ρ_0 . Note that these values agree approximately with those obtained in a recent refined hadronic model [3] .

2. 'Dropping' vector meson mass

In order to explore the observable consequences of vector meson mass shifts at finite nuclear density the in-medium vector meson masses are modelled according to Hatsuda and Lee [4] or Brown/Rho scaling [1] as

$$m_V^* = m_V(1 - \alpha \rho_N(r)/\rho_0), \quad (19)$$

where $\rho_N(r)$ is the nuclear density at the resonance decay, $\rho_0 = 0.16 \text{ fm}^{-3}$ and $\alpha \simeq 0.18$ for the ρ and ω . The latter value of α has also been used in Refs. [22,23] and led to a good description of the dilepton spectra from the CERES and HELIOS-3 Collaborations. Furthermore, in Ref. [3] a shift of the ω pole by ≈ 120 MeV is reported, however, no essential

shift of the ρ -meson pole is extracted from their dynamical calculations (cf. also Ref. [51]). Thus the parameter α in (19) has to be taken with same care and finally to be determined by experiment.

3. The ρ spectral function

While the dropping mass scenario, together with the collisional broadening, reproduces, at least qualitatively, the results of the more refined model of Ref. [3], it is an oversimplified approximation for the ρ -meson. For the ρ -meson we, therefore, also include alternatively the calculated spectral function from Ref. [13]. The implementation of the ρ spectral function into the transport approach for the calculation of the dilepton yield from ρ^0 decay is described in Refs. [25,26]. Here we adopt the same strategy, i.e. the dilepton radiation from ρ mesons is calculated as

$$\frac{dN_{\rho \rightarrow l^+ l^-}}{dM} = -Br(M) \frac{2M}{\pi} \text{Im} D_\rho(q_0, q; \rho_N), \quad (20)$$

where D_ρ is the ρ -meson propagator [13] in the hadronic medium depending on the baryon density ρ_N as well as on energy q_0 and 3-momentum $q \equiv |\mathbf{q}|$ in the local rest frame of the baryon current ('comoving' frame). The invariant mass M is related to the ρ -meson 4-momentum in the nuclear medium as $M^2 = q_0^2 - q^2$, while $\text{Im} D_\rho$ is spin averaged over the longitudinal and transverse part of the ρ -propagator [13]. Furthermore, $Br(M)$ is the branching ratio of the ρ -meson resonance to dileptons which is in principle an explicit function of the invariant mass M . Vector-Meson-Dominance can not be used to evaluate this function where a large part of the ρ -strength resides in nucleon resonance-hole excitations [13]. For the nucleon resonances the simple VDM is known to be quite inaccurate [11]. In the absence of any detailed study of this problem, we have used a constant branching ratio fixed at the resonance mass for simplicity as in [25,26]; in future this simplifying assumption will have to be improved.

IV. DILEPTONS FROM π A REACTIONS

We now come to the results of our numerical simulations. In Fig. 5 we present the calculated dilepton invariant mass spectra $d\sigma/dM$ for π^- Pb at the bombarding energy of $E_{kin} = 1.3$ GeV including a finite mass resolution of 10 MeV. The upper part corresponds to the result calculated without collisional broadening and free meson masses. The middle part shows the dilepton spectra calculated including the collisional broadening effect and ‘dropping’ masses of ρ and ω mesons (Eq. (19)), whereas the lower part corresponds to calculations with collisional broadening and dropping mass shift for the ω -meson and the momentum- and density-dependent spectral function [13] (Eq. (20)) for the ρ -meson.

The thin lines indicate the individual contributions from the different production channels; *i.e.* starting from low M : Dalitz decay $\eta \rightarrow \gamma e^+ e^-$ (dotted line), $\Delta \rightarrow N e^+ e^-$ (short-dotted line), $\omega \rightarrow \pi^0 e^+ e^-$ (dot-dashed line), $N(1520) \rightarrow N e^+ e^-$ (dot-dashed line), $N(1535) \rightarrow N e^+ e^-$ (long-dashed line); for $M \approx 0.8$ GeV: $\omega \rightarrow e^+ e^-$ (dashed line), $\rho^0 \rightarrow e^+ e^-$ (dot-dashed line). The full solid line represents the sum of all sources considered here.

The dominant background processes in the low mass region up to $M \simeq 500$ MeV are the η and ω Dalitz decays and possibly πN bremsstrahlung, which is discarded here. The contributions from heavy-baryon resonances are negligibly small. Above $M \sim 0.6$ GeV the spectrum is dominated by the vector meson decays with a low background from other hadronic sources. Our results are in qualitative agreement with the INC calculations in Refs. [28,29] but differ in the individual channels by up to factors of 2 which is due to the use of different elementary cross sections as mentioned already at the end of section A and to the explicit treatment of isospin in our transport approach.

As seen from the middle part, the mass shift and the collisional broadening effect leads to a two-component structure for the ω meson: the narrow peak at $M = m_\omega$ comes from the ω decaying outside the nucleus whereas the broader peak corresponds to the decay inside the nucleus. For the ρ meson this effect is not seen because the ρ mesons practically all

decay inside the nucleus due to their short lifetime; only the width of the ρ meson peak becomes larger due to collisional broadening. The 'dropping' mass for the ρ and ω mesons leads to an essential reduction of the vector meson production threshold in meson-baryon and baryon-baryon collisions and to a slight enhancement of vector meson production in pion-nucleus collisions. A similar effect is seen if one employs the ρ spectral function (lower part in Fig. 5) instead of a dropping ρ -mass.

We have also performed calculations for light systems (in order to test different density regimes) and two incoming energies. In Figs. 6 and 7 we show the dilepton invariant mass spectra $d\sigma/dM$ for π^-C , π^-Ca and π^-Pb at the bombarding energies of $E_{kin} = 1.3$ and 1.7 GeV, respectively. The solid lines indicate the sum of all dilepton channels calculated without collisional broadening and with 'free' meson masses. The dotted lines are the results with collisional broadening and a 'dropping' mass of ρ and ω mesons. The dashed lines correspond to calculations with collisional broadening, with dropping ω mass and with the ρ spectral function [13]. The 'dropping mass' scheme leads to an enhancement by about a factor 2 as compared to the free meson mass in the dilepton range $0.6 \leq M \leq 0.7$ GeV and to a reduction by about a factor of 2 above the ω peak. The ρ spectral function also slightly enhances the yield at $0.6 \leq M \leq 0.7$ GeV, however, the reduction above the ω peak is not so strong as compared to the 'free' meson mass case. As seen from Figs. 6 and 7 the difference between the three scenarios exists even for a light system like ^{12}C and becomes more pronounced for heavy nuclei like ^{208}Pb due to the larger volume.

In Fig. 8 we present the same analysis as in Fig. 7, but the dilepton spectra were calculated including a cut in the longitudinal momentum of the dileptons, i.e. $q_z \leq 0.3$ GeV/c, which makes the differences between the 'dropping mass' scheme and the ρ spectral function more pronounced. Fig. 8 demonstrates that with a proper q_z cut one should be able to distinguish experimentally between the two scenarios for the medium modifications of the vector mesons.

V. SUMMARY

On the basis of the Coupled-Channel-BUU approach (CBUU) [30] we have studied dilepton production in π^-C , π^-Ca and π^-Pb collisions at $E_{kin} = 1.3$ and 1.7 GeV. Various contributions are taken into account for dilepton production: the Dalitz-decays of Δ , $N(1440)$, $N(1520)$, $N(1535)$ resonances and η, ω mesons as well as the direct dilepton decays of the vector mesons ρ and ω .

The contributions from vector mesons were calculated including the collisional broadening and by applying two different in-medium modification schemes of the vector mesons: i) the dropping mass and ii) the hadronic spectral function approach [13].

It was found that both scenarios lead to an enhancement of the dilepton yield at $0.6 \leq M \leq 0.77$ GeV. However, the models predict quite different absolute values for the dilepton yield at invariant masses mainly below and above $M = m_V$ with the total in-medium effect amounting up to a factor of 3. This sensitivity, which is comparable to that achieved in heavy-ion reactions [25], can be studied experimentally especially after applying proper longitudinal momentum cuts and comparing directly the spectra from light and heavy targets such as ^{12}C or ^{208}Pb .

ACKNOWLEDGMENTS

The authors are grateful for various discussions with H. Bokemeyer, Ye.S. Golubeva, W. Koenig, L.A. Kondratyuk, W. Kühn, V. Metag, W. Schön and A. Sibirtsev. Furthermore, they are indebted to M. Post and W. Peters for the ρ spectral function from Ref. [13].

REFERENCES

- [1] G.E. Brown and M. Rho, Phys. Rev. Lett. **66**, 2720 (1991).
- [2] C.M. Shakin and W.-D. Sun, Phys. Rev. **C 49**, 1185 (1994).
- [3] F. Klingl and W. Weise, Nucl. Phys. **A606**, 329 (1996); F. Klingl, N. Kaiser and W. Weise, Nucl. Phys. **A624**, 527 (1997).
- [4] T. Hatsuda and S. Lee, Phys. Rev. **C 46**, R34 (1992).
- [5] M. Asakawa and C.M. Ko, Phys. Rev. **C 48**, R526 (1993).
- [6] S. Leupold, W. Peters and U. Mosel, Nucl. Phys. **A628**, 311 (1998).
- [7] M. Herrmann, B. Friman, and W. Nörenberg, Nucl. Phys. **A560**, 411 (1993).
- [8] M. Asakawa, C. M. Ko, P. Lévai, and X. J. Qiu, Phys. Rev. **C 46**, R1159 (1992).
- [9] G. Chanfray and P. Schuck, Nucl. Phys. **A545**, 271c (1992).
- [10] R. Rapp, G. Chanfray, and J. Wambach, Phys. Rev. Lett. **76**, 368 (1996).
- [11] B. Friman and H. J. Pirner, Nucl. Phys. **A617**, 496 (1997).
- [12] R. Rapp, G. Chanfray and J. Wambach, Nucl. Phys. **A617**, 472 (1997).
- [13] W. Peters, M. Post, H. Lenske, S. Leupold, and U. Mosel, Nucl. Phys. **A632**, 109 (1998).
- [14] L. A. Kondratyuk, M. Krivoruchenko, N. Bianchi, E. De Sanctis and V. Muccifora, Nucl. Phys. **A579**, 453 (1994).
- [15] K. G. Boreskov, J. Koch, L. A. Kondratyuk and M. I. Krivoruchenko, Phys. of Atomic Nuclei **59**, 1908 (1996).
- [16] G. Agakichiev et al., Phys. Rev. Lett. **75**, 1272 (1995).
- [17] Th. Ullrich et al., Nucl. Phys. **A610**, 317c (1996); A. Drees, Nucl. Phys. **A610**, 536c

- (1996).
- [18] M. A. Mazzoni, Nucl. Phys. **A566**, 95c (1994); M. Masera, Nucl. Phys. **A590**, 93c (1995).
 - [19] T. Åkesson et al., Z. Phys. **C 68**, 47 (1995).
 - [20] G. Q. Li, C. M. Ko, and G. E. Brown, Phys. Rev. Lett. **75**, 4007 (1995).
 - [21] C. M. Ko, G. Q. Li, G. E. Brown, and H. Sorge, Nucl. Phys. **A610**, 342c (1996).
 - [22] W. Cassing, W. Ehehalt, and C. M. Ko, Phys. Lett. **B 363**, 35 (1995).
 - [23] W. Cassing, W. Ehehalt, and I. Kralik, Phys. Lett. **B 377**, 5 (1996).
 - [24] E. L. Bratkovskaya and W. Cassing, Nucl. Phys. **A619**, 413 (1997).
 - [25] W. Cassing, E. L. Bratkovskaya, R. Rapp, and J. Wambach, Phys. Rev. **C 57**, 916 (1998).
 - [26] E. L. Bratkovskaya, W. Cassing, R. Rapp, and J. Wambach, Nucl. Phys. **A634**, 168 (1998).
 - [27] W. Schön, H. Bokemeyer, W. Koenig, and V. Metag, Acta Physica Polonica **B 27**, 2959 (1996).
 - [28] W. Cassing, Ye. S. Golubeva, A. S. Iljinov, and L. A. Kondratyuk, Phys. Lett. **B 396**, 26 (1997).
 - [29] Ye. S. Golubeva, L. A. Kondratyuk and W. Cassing, Nucl. Phys. **A625**, 832 (1997).
 - [30] S. Teis, W. Cassing, M. Effenberger, A. Hombach, U. Mosel, and Gy. Wolf, Z. Phys. **A 356**, 421 (1997); Z. Phys. **A 359**, 297 (1997).
 - [31] G. F. Bertsch and S. Das Gupta, Phys. Rep. **160**, 189 (1988).
 - [32] W. Cassing, K. Niita and S. J. Wang, Z. Phys. **A 331**, 439 (1988).

- [33] W. Cassing, V. Metag, U. Mosel and K. Niita, Phys. Rep. **188**, 363 (1990).
- [34] K. Weber, B. Blättel, W. Cassing, H.-C. Dönges, V. Koch, A. Lang and U. Mosel, Nucl. Phys. **A539**, 713 (1992); K. Weber, B. Blättel, W. Cassing, H.-C. Dönges, A. Lang, T. Maruyama and U. Mosel, Nucl. Phys. **A552**, 571 (1993).
- [35] G. Welke, M. Prakash, T. T. S. Kuo and S. Das Gupta, Phys. Rev. **C 38**, 2101 (1988).
- [36] B. A. Li, Z. Z. Ren, C. M. Ko, and S. Y. Yennello, Phys. Rev. Lett. **76**, 4492 (1996).
- [37] Review of Particle Properties: Phys. Rev. **D 50** (1994).
- [38] Baldini et al., *Landolt-Börnstein* vol. 12, Springer, Berlin (1987)
- [39] W. Cassing and U. Mosel, Prog. Part. Nucl. Phys. **25**, 235 (1990).
- [40] Gy. Wolf, G. Batko, W. Cassing, U. Mosel, K. Niita, and M. Schäfer, Nucl. Phys. **A517**, 615 (1990); Gy. Wolf, W. Cassing and U. Mosel, Nucl. Phys. **A552**, 549 (1993).
- [41] T. Vetter, A. Engel, T. Biro and U. Mosel, Phys. Lett. **B 263**, 153 (1991).
- [42] H. Calén et al., Phys. Lett. **B 366**, 39 (1996); Phys. Rev. Lett. **79**, 2642 (1997); Phys. Rev. Lett. **80**, 2069 (1998).
- [43] J. Cugnon, P. Deneye and J. Vandermeulen, Phys. Rev. **C 41**, 1339 (1990).
- [44] A. Sibirtsev, W. Cassing and U. Mosel, Z. Phys. **A 358**, 357 (1997).
- [45] A. Sibirtsev and W. Cassing, Nucl. Phys. **A629**, 707 (1998).
- [46] E. Chiavassa et al., Phys. Lett. **B 322**, 270 (1994); **B 337**, 192 (1994).
- [47] C. Gale and J. Kapusta, Phys. Rev. **C 40**, 2397 (1989).
- [48] M. Schäfer, T. S. Biro, W. Cassing, and U. Mosel, Phys. Lett. **B 221**, 1 (1989).
- [49] P. Lichard, Phys. Rev. **D 51**, 6017 (1995).
- [50] H. C. Eggers, C. Gale, R. Tabti, and K. Haglin, hep-ph/9604372; Phys. Rev. **D 53**,

4822 (1996).

- [51] L. A. Kondratyuk, A. Sibirtsev, W. Cassing, Ye. S. Golubeva, and M. Effenberger, Phys. Rev. **C 58**, 1078 (1998).

FIGURES

FIG. 1. The binding energy per nucleon as a function of the nucleus mass number. The solid curve corresponds to the binding energy calculated with the symmetry potential U^{symm} whereas the dashed curve is the result of a calculation without U^{symm} . The dotted line corresponds to the empirical values according to the liquid drop formula.

FIG. 2. The calculated total $\pi^- - p$ -cross section in comparison to the data from [38] (solid line). The dot-dot-dashed, the dot-dashed and the short-dashed lines show the contributions from the $\Delta(1232)$, the $N(1440)$ and the $N(1520)$ separately. The long-dashed line indicates the contribution of the additional two pion production channel.

FIG. 3. The distribution in the pion-baryon collision number versus the invariant energy \sqrt{s} above the threshold for ρ production $\sqrt{s_0} = m_N + m_\rho$, i.e. $dN/d\sqrt{s}$ (histogram), for π^- -Pb at $E_{kin} = 1.3$ GeV. The arrow indicates the incoming energy.

FIG. 4. The width of the ρ and ω mesons calculated according to Eqs. (15),(16) (open squares) for π^- -Pb at $E_{kin} = 1.3$ GeV. The solid lines indicate a linear fit with density according to Eq. (18).

FIG. 5. The dilepton invariant mass spectra $d\sigma/dM$ for π^- -Pb at the bombarding energy of $E_{kin} = 1.3$ GeV calculated without collisional broadening and with free meson masses (upper part), including the collisional broadening effect and a 'dropping' mass of the ρ and ω mesons (middle part) as well as including the ρ spectral function from Ref. [13] instead of a 'dropping' ρ -mass (lower part). The thin lines indicate the individual contributions from the different production channels; *i.e.* starting from low M : Dalitz decay $\eta \rightarrow \gamma e^+ e^-$ (dotted line), $\Delta \rightarrow N e^+ e^-$ (short-dotted line), $\omega \rightarrow \pi^0 e^+ e^-$ (dot-dashed line), $N(1520) \rightarrow N e^+ e^-$ (dot-dashed line), $N(1535) \rightarrow N e^+ e^-$ (long-dashed line); for $M \approx 0.8$ GeV: $\omega \rightarrow e^+ e^-$ (dashed line), $\rho^0 \rightarrow e^+ e^-$ (dot-dashed line). The full solid line represents the sum of all sources.

FIG. 6. The dilepton invariant mass spectra $d\sigma/dM$ for π^-C , π^-Ca and π^-Pb at the bombarding energy of $E_{kin} = 1.3$ GeV. The solid lines indicate the sum of all dilepton channel calculated without collisional broadening and with free meson masses. The dotted curves are the result with collisional broadening and 'dropping' masses of ρ and ω mesons. The dashed curves correspond to the calculations with collisional broadening, dropping ω mass and with the ρ spectral function from Ref. [13].

FIG. 7. The dilepton invariant mass spectra $d\sigma/dM$ for π^-C , π^-Ca and π^-Pb at the bombarding energy of $E_{kin} = 1.7$ GeV. The assignment is the same as in Fig. 6.

FIG. 8. The dilepton invariant mass spectra $d\sigma/dM$ for π^-C , π^-Ca and π^-Pb at the bombarding energy of $E_{kin} = 1.7$ GeV with a longitudinal momentum cut $q_z \leq 0.3$ GeV/c. The assignment is the same as in Fig. 6.

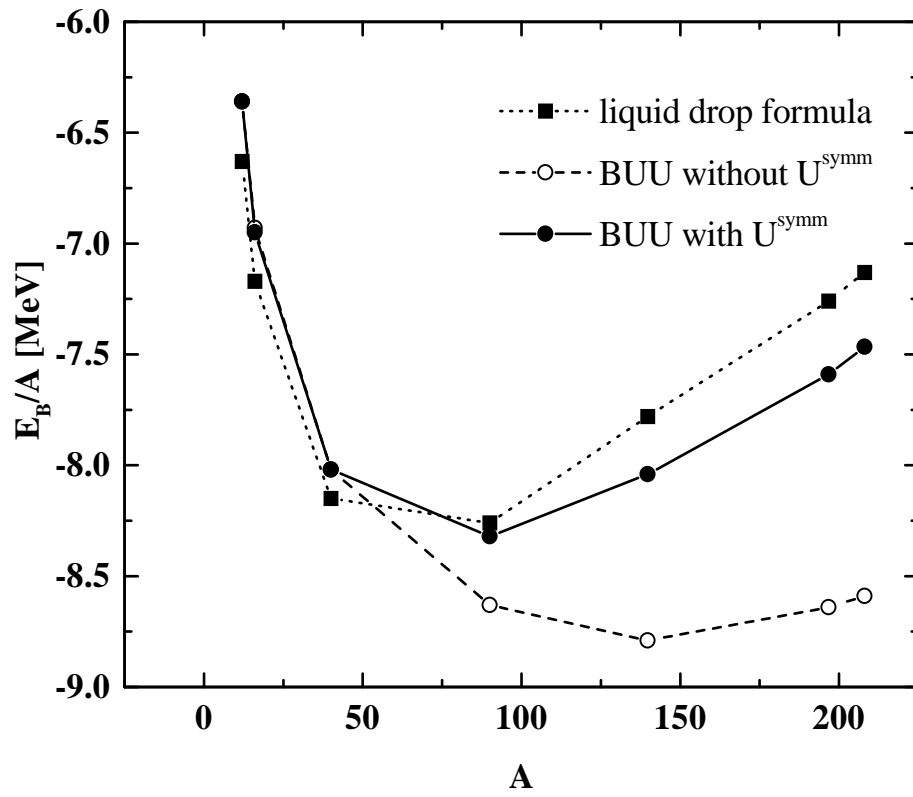


Fig. 1

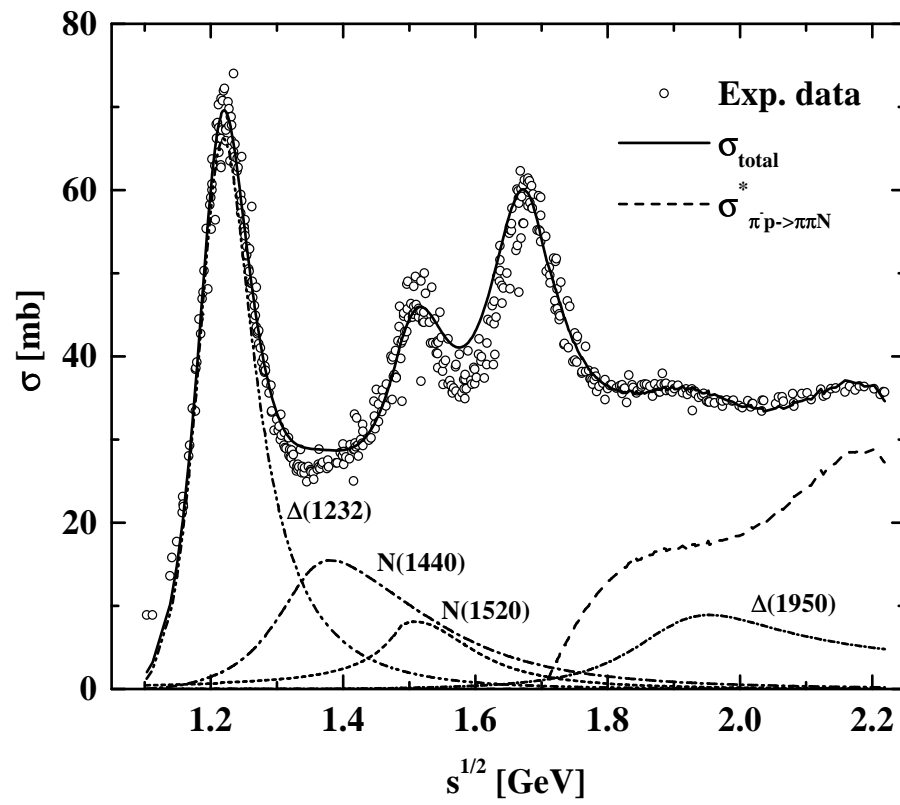


Fig. 2

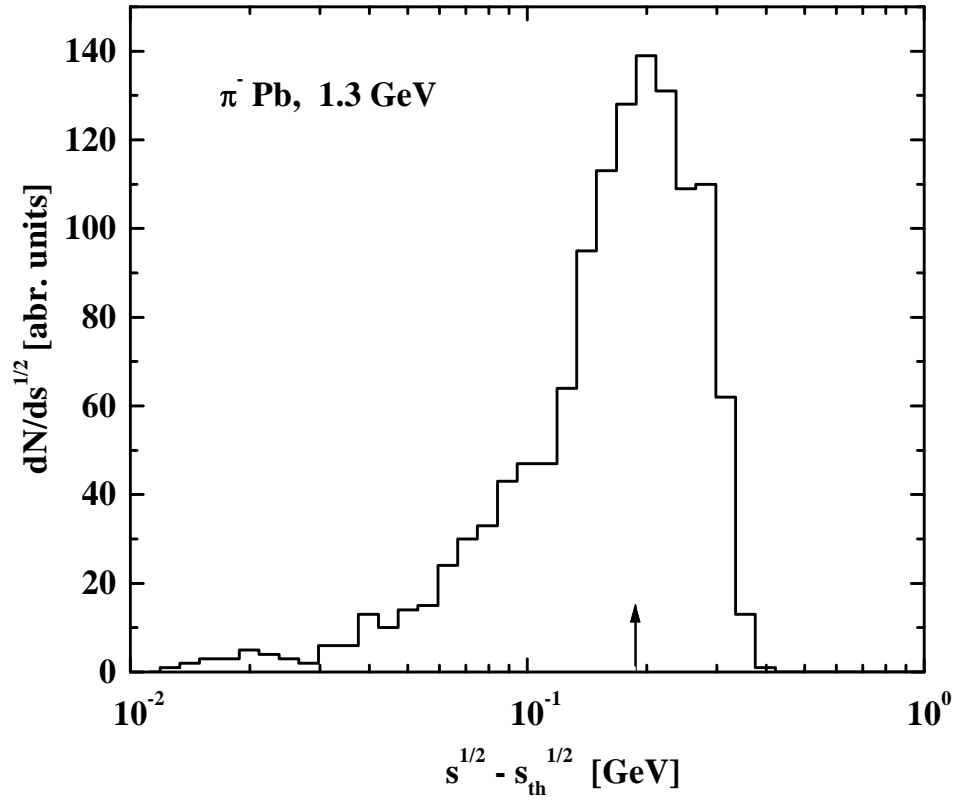


Fig. 3

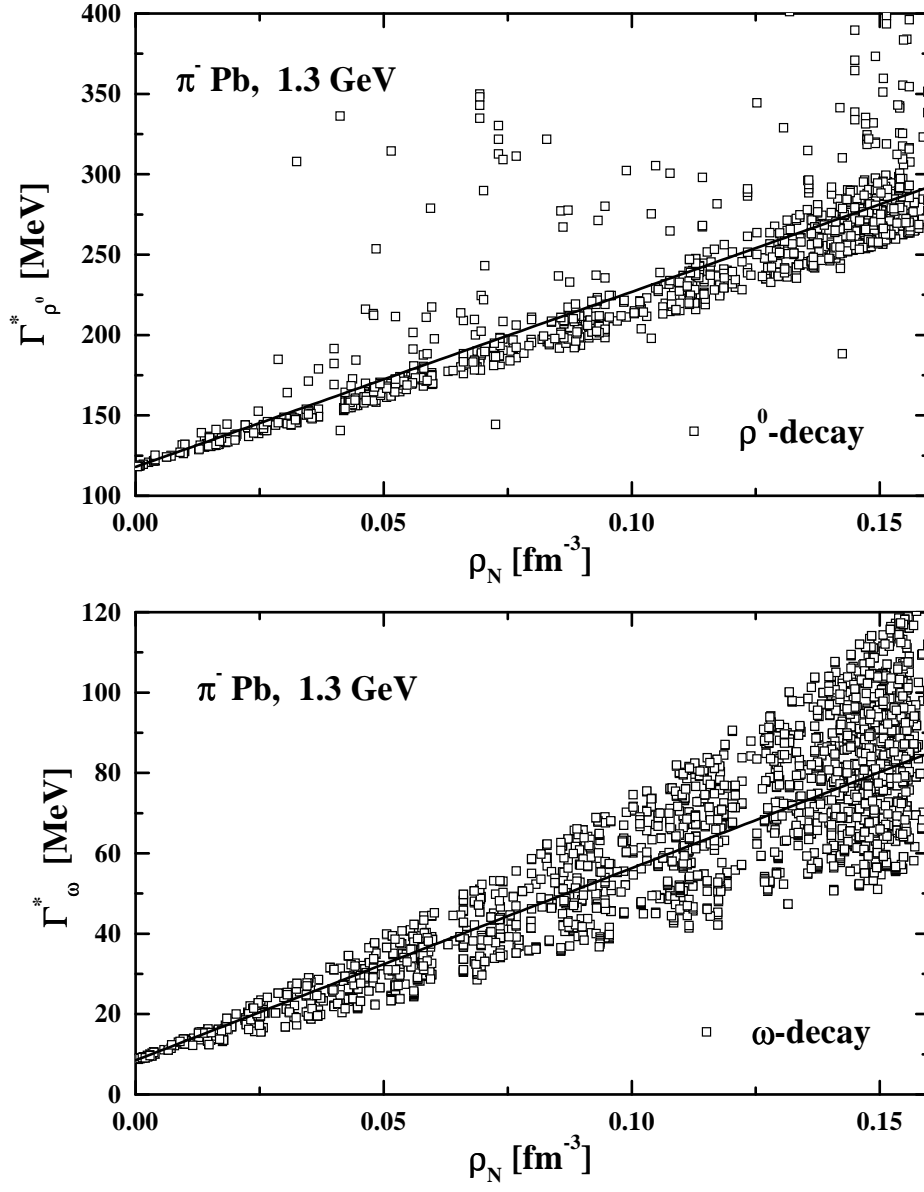


Fig. 4

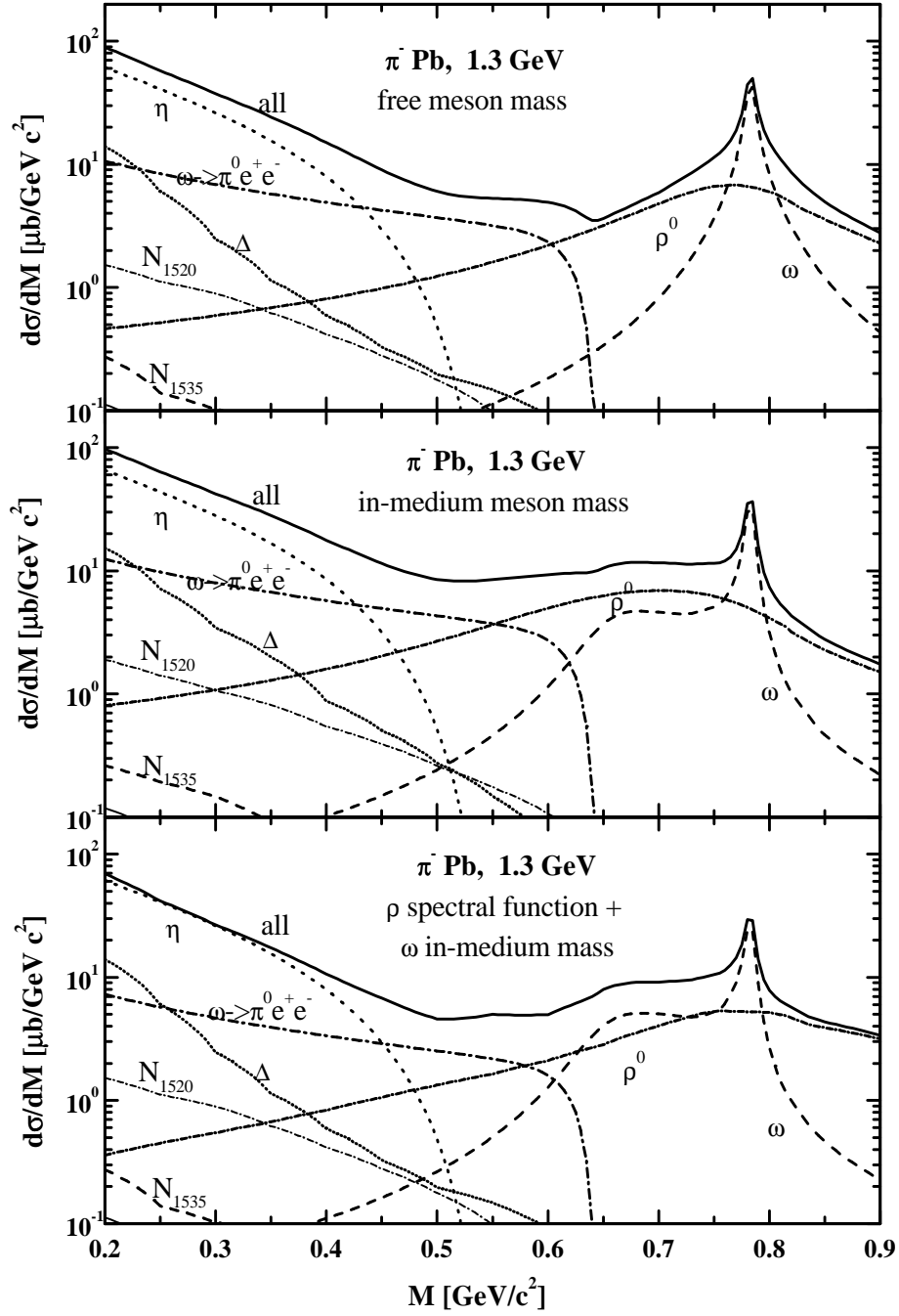


Fig. 5

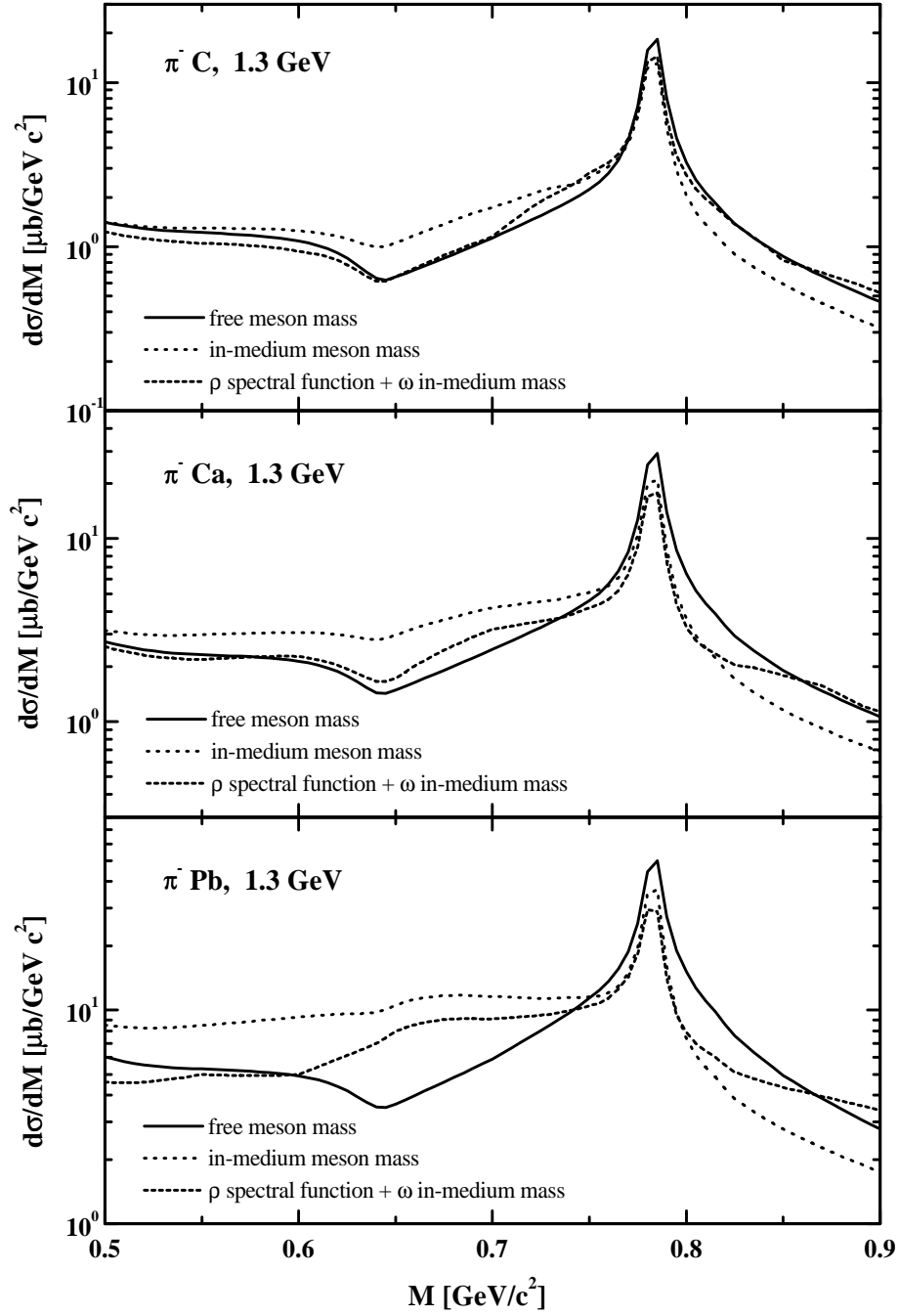


Fig. 6

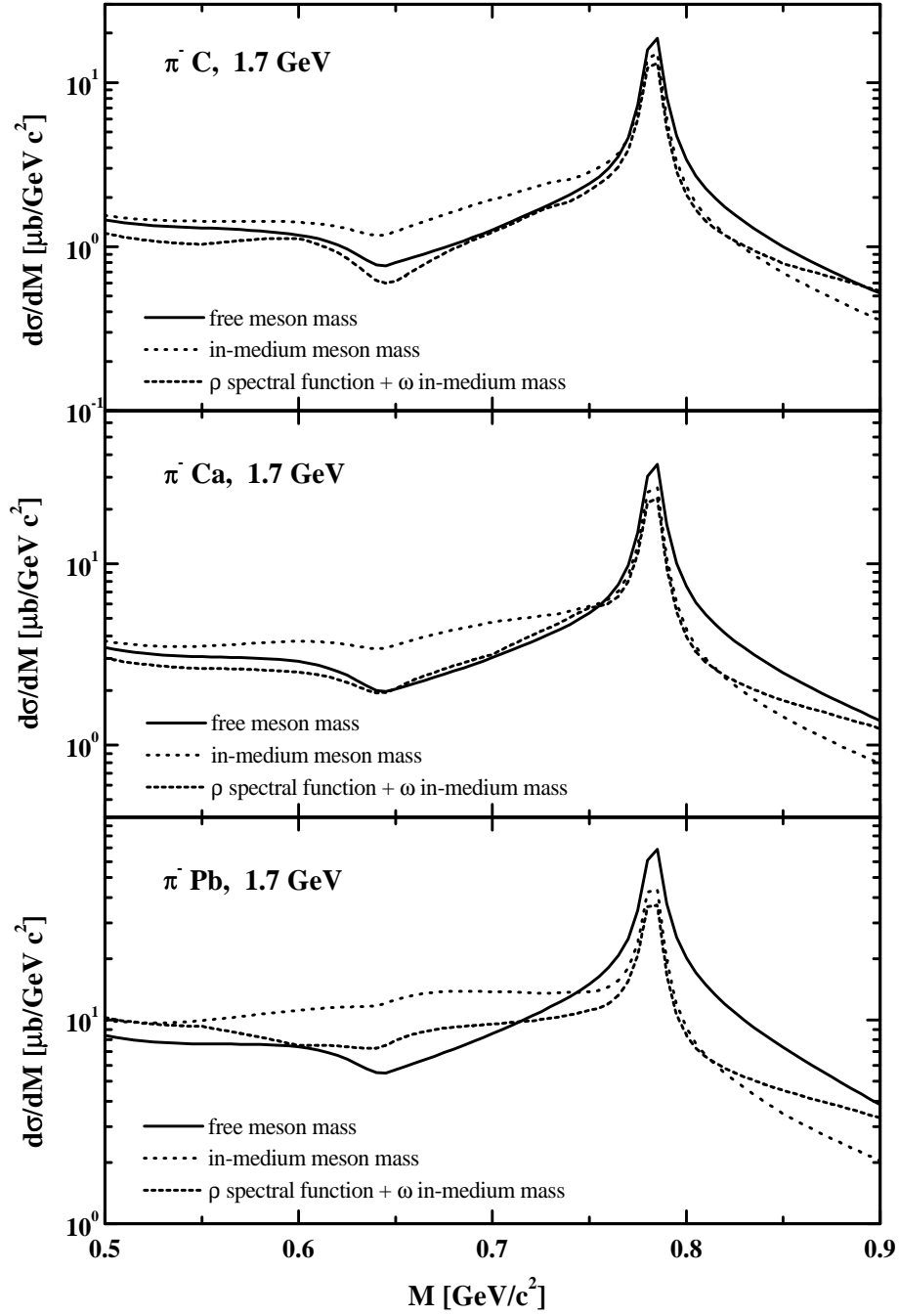


Fig. 7

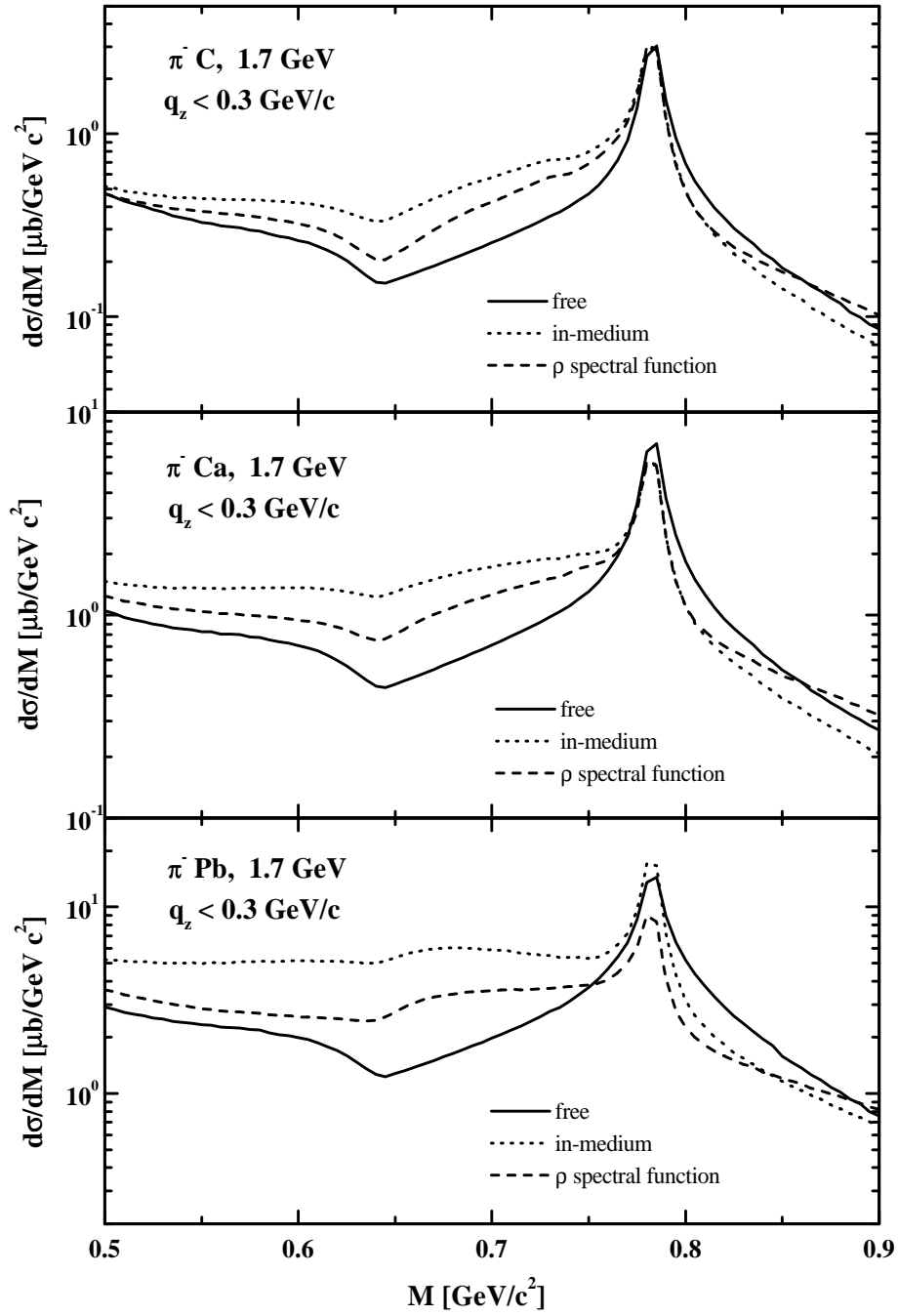


Fig. 8